crystals

MDPI

Article

Chitosan–Alginate Nanocontainers with Caffeine as Green Corrosion Inhibitors for Protection of Galvanized Steel

Kamelia Kamburova [1], Nelly Boshkova [1], Tsetska Radeva [1], Maria Shipochka [2] and Nikolai Boshkov [1,*]

[1] Institute of Physical Chemistry "R. Kaishev", Bulgarian Academy of Sciences, "Acad. G. Bonchev" St. Bl. 11, 1113 Sofia, Bulgaria; kamelia@ipc.bas.bg (K.K.); nelly.boshkova@ipc.bas.bg (N.B.); radeva@ipc.bas.bg (T.R.)
[2] Institute of General and Inorganic Chemistry, Bulgarian Academy of Sciences, "Acad. G. Bonchev" St. Bl. 11, 1113 Sofia, Bulgaria; shipochka@svr.igic.bas.bg
* Correspondence: nboshkov@ipc.bas.bg

Abstract: The introduction of new regulations needs to develop eco-friendly systems to prevent corrosion. In this work, a natural corrosion inhibitor caffeine (CAF) was encapsulated in polysaccharide-based nanoparticles, capable of the responsive release of CAF during corrosion. The nanoparticles were prepared using electrostatic complexation between two natural polysaccharides which are oppositely charged—chitosan (CHI) and sodium alginate (ALG), crosslinked by tripolyphosphate (TPP). The particle size distribution and zeta potential were evaluated using dynamic light scattering and laser Doppler velocimetry. The encapsulation efficiency and release of CAF from nanocontainers was evaluated with UV-spectroscopy. The nanoparticles were incorporated via electrodeposition into the zinc coating on low-carbon steel to ensure self-healing. Cyclic voltammetry demonstrated the cathodic and anodic processes in the starting electrolytes. Surface hydrophobicity was investigated by water contact angle (WCA). The corrosion resistance of the coatings was estimated with polarization resistance (Rp) measurements and potentiodynamic polarization (PDP) curves. The study of the chemical composition of the coatings was carried out with X-ray photoelectron spectroscopy. The data obtained confirm the indisputable influence of the nanoparticles/nanocontainers on the protective feature of the hybrids—the latter have about twice-higher Rp values compared to the ordinary zinc.

Keywords: chitosan; alginate; caffeine; nanocontainers; corrosion; inhibitor; hybrid coatings

check for updates

Citation: Kamburova, K.; Boshkova, N.; Radeva, T.; Shipochka, M.; Boshkov, N. Chitosan–Alginate Nanocontainers with Caffeine as Green Corrosion Inhibitors for Protection of Galvanized Steel. *Crystals* **2024**, *14*, 660. https://doi.org/10.3390/cryst14070660

Academic Editors: Jijo Christudasjustus, Rajeev Gupta, Mohammad Umar Farooq Khan and Ulises Martin Diaz

Received: 28 June 2024
Revised: 15 July 2024
Accepted: 16 July 2024
Published: 19 July 2024

Copyright: © 2024 by the authors. Licensee MDPI, Basel, Switzerland. This article is an open access article distributed under the terms and conditions of the Creative Commons Attribution (CC BY) license (https://creativecommons.org/licenses/by/4.0/).

1. Introduction

The electrodeposition of zinc on the surface of steel materials is one of the most extensive techniques for ensuring a sacrificial protection and barrier effect against steel corrosion in aggressive media. The disruption of this metal in a corrosion medium with neutral pH containing Cl^--ions results in the appearance of a layer of corrosion products with a low solubility value (hydroxides, hydroxide chlorides, oxides, etc.) on the surface [1–3]. This layer plays the role of a physical barrier and makes the access of corrosive species to the surface of the metal difficult, protecting and enhancing in such a way the lifetime of the metal. However, once microdefects are formed in the coating, the latter will begin to lose its barrier properties. The addition of a corrosion inhibitor to the coating can heal the microdefects, which will ensure the prevention of the corrosive media from reaching the coating/steel interface. The direct addition of the inhibitor can cause adverse effects due to its possible reaction with the metal substrate in advance [4]. Encapsulation of the corrosion inhibitor into micro- or nanocarriers is a good way to avoid the above drawbacks, offering an inhibitor release on demand for better protection of the substrate (self-healing effect) [5–8]. The release of the corrosion inhibitor at the right moment is a key to the long-term protection of the coating. For example, the encapsulation of the corrosion inhibitor in pH-sensitive nanocarriers is expected to reduce the corrosion rate in the case of local changes in pH during a corrosion attack.

Scientists have been forced to use natural and biodegradable inhibitors for metal protection in different media due to the serious hazards of chemical inhibitors [9]. Caffeine, a naturally derived nontoxic and environmentally friendly alkaloid (Figure 1), demonstrates well-expressed properties of an effective corrosion inhibitor, having oxygen and nitrogen heteroatoms, π-electrons, and polar functions that are centers for adsorption on metal substrates [10]. The application of CAF in the role of an inhibitor against corrosion has been evaluated for different metals including steel [11,12], zinc [13], and copper [14]. Due to a synergistic effect that contributed to the formation of a protective film containing the Fe^{2+}–caffeine complex and $Zn(OH)_2$, caffeine has also been demonstrated to have an excellent inhibition efficiency for mild steel in the presence of Zn^{2+} cations [15].

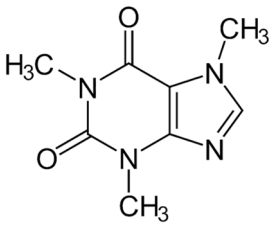

Figure 1. Structural scheme of caffeine.

In recent years, wide applications have found materials made from polysaccharides as a "green" option to synthetic polymers due to their nontoxicity, biocompatibility, and biodegradability. Polysaccharide complexes of chitosan and alginate have been extensively applied and studied [16,17]. Chitosan is a cationic polysaccharide consisting of β-(1,4)-linked 2-deoxy-2-amino-D-glucopyranose units, derived from chitin by alkaline deacetylation. It has been applied in many industries like engineering, food, pharmaceutical, biomedical, chemical, and agricultural industries [18]. Alginate is an anionic polysaccharide, consisting of blocks of two uronic acids—α-Lguluronic acid and ß-L-mannuronic acid. It is obtained predominantly from the cell walls of brown algae. Alginate has also found applications in biomedical, pharmaceutical, agricultural, and tissue-engineering industries [19]. Both polysaccharides have been studied as inhibitors against the corrosion of steel since they contain nitrogen and oxygen atoms in the structures of their molecules. For example, CHI and ALG have been found to increase significantly the anticorrosion properties of steel in HCl and in 3.5% NaCl solutions [20,21].

Chitosan and alginate are weak polyelectrolytes that can form complexes (hydrogel particles) as a result of electrostatic interaction between the positively charged amino (NH_3^+) groups of chitosan and negatively charged carboxylic (COO^-) groups of alginate. Stable compact structures of CHI/ALG complexes were realized mainly at pH $\geq$ 5 [22,23]. The important feature of such complexes is that they swell in response to the surrounding pH changes, as the charge imbalance lowers the attraction between the oppositely charged polysaccharide molecules [23,24].

The scientific literature contains information concerning the zinc coatings which are widely used in the field of corrosion protection (mainly of low-carbon steel), since their electrochemical potential [25–27] is more negative compared to the iron. Zinc demonstrates a sacrificial action because in a corrosive environment its surface is overlaid by newly formed products with low solubility which slow down the disruptive influence of the aggressive ions [28]. The newly formed corrosion products demonstrate the role of a physical protective barrier. Obviously, zinc is the anode when in contact with iron providing the sacrificial protection. Many zinc coating types on steel have been elaborated and studied: electroplated, thermally sprayed, hot-dip galvanized coatings applied to steel surfaces, as well as those painted with zinc-rich coatings [25].

Nowadays, the widely applied practice is to replace the ordinary zinc coatings with composite or hybrid ones [25,28]. For example, the embedding of different inorganic or organic/polymeric particles enhances the protective characteristics of the ordinary zinc coatings [29–34]. The incorporated particles fill some of the microdefects, the latter

acting as active sites for corrosion development, and minimize the development of the corrosion process. Generally, the incorporated particles participate in the formation process of "mixed" barrier layers simultaneously containing corrosion products with low solubility and embedded particles.

CHI/ALG-based nanomaterials have found applications in different fields due to their loading ability. CHI/ALG nanoparticles (with a hydrogel character) loaded with CAF are prepared using polyelectrolyte complexation in the presence of sodium tripolyphosphate which is a crosslinking agent (TPP). The resulting CHI/ALG nanoparticles are electrodeposited with zinc on a cathode (low-carbon steel) surface from a slightly acidic zinc sulfate solution. The protective properties of the obtained hybrid coating are compared to those of the ordinary zinc coating and a zinc coating containing CHI/ALG nanoparticles unloaded with caffeine.

In the present work, the encapsulation of CAF in CHI/ALG nanoparticles is applied for the obtaining of environmentally friendly nanocarriers, capable of a pH-responsive release of CAF in a zinc coating, aiming to improve the corrosion protection of mild steel in aggressive chloride media. To the best of our knowledge, the synthesis of environmentally friendly nanocontainers with CAF and their application for the improvement of the corrosive protection of metallic coatings on steel are still lacking.

2. Materials and Methods

2.1. Materials

Chitosan (Mw~50–190 kDa) with a degree of deacetylation (75–85%), sodium alginate (Mw~30–100 kDa), sodium tripolyphosphate, caffeine, acetic acid, and sodium hydroxide of analytical grade were purchased from Sigma Aldrich (Darmstadt, Germany). The stock solution of CHI with a concentration of 1 g/L was prepared by magnetic stirring for 24 h in 0.03 M acetic acid, and the pH of the solution was adjusted to 5.0 using NaOH. Stock solutions of ALG and CAF with concentrations of 1 g/L were obtained by magnetic stirring for 30 min in double-distilled water. Analytical-grade chemicals for electrodeposition of the hybrid zinc coatings, i.e., $ZnSO_4 \cdot 7H_2O$, NH_4Cl, and H_3BO_3, were supplied by Valerus Ltd., Sofia, Bulgaria.

2.2. Preparation of CHI/ALG Nanoparticles

CHI/ALG nanoparticles unloaded with CAF were obtained according to a previously described procedure with slight modification [35–37]. Briefly, 20 mL of ALG solution (0.45 g/L) and a 20 mL solution of sodium TPP (1 g/L) were mixed and added to 100 mL of CHI solution by applying magnetic stirring for 30 min in order to obtain a weight ratio of 11:1 for CHI and ALG and a ratio of 5:1 for CHI and TPP, respectively. The obtained suspension was homogenized by sonication for 1 min. Using the same procedure, CHI/ALG nanoparticles were loaded with CAF (1 g/L) by mixing CAF with the ALG-TPP solution before adding to the CHI solution.

2.3. Characterization of CHI/ALG Nanoparticles

The size distribution and surface charge density of the CHI/ALG nanoparticles, both unloaded and loaded with CAF, were evaluated using dynamic light scattering (DLS) and laser Doppler velocimetry (Zetasizer Pro Red Label, Malvern Panalytical Ltd., Malvern, UK) measurements. The mean size (hydrodynamic diameter) and zeta (ζ) potential of both types of nanoparticles were measured in aqueous solutions at pH 5.0. As a light source, a He-Ne laser was used, and the intensity of the scattered light was measured by a detector at 173°.

2.4. Zinc Coating Electrodeposition on Low-Carbon Steel Substrates

Present investigations were realized with test samples of ordinary zinc and two types of hybrid zinc coatings. Low-carbon steel lamellas with sizes of 2 cm × 1 cm × 0.1 cm were used as substrates. The composition of the starting electrolytes was 150 g/L $ZnSO_4 \cdot 7H_2O$,

30 g/L NH_4Cl, and 30 g/L H_3BO_3. Furthermore, two kinds of additives were applied—wetting agent AZ1 (50 mL/L, IPC-BAS, Sofia, Bulgaria) and brightener AZ2 (2 mL/L, IPC-BAS, Sofia, Bulgaria). The experimental pH value of the starting electrolytes was 4.5–5.0. The electrodeposition was held in a glass cell (volume 600 mL) at room temperature, with a cathode current (direct current) density of 2 A/dm^2 and the application of metallurgical zinc anodes. The obtained two types of hybrid coating types were marked as follows:

- CS—hybrid zinc coatings with incorporated nanoparticles;
- CS CAF—hybrid coatings with incorporated nanocontainers loaded with caffeine.

For the comparison of the most important electrochemical characteristics, ordinary zinc coatings were also obtained from a solution having a composition of 150 g/L $ZnSO_4 \cdot 7H_2O$, 30 g/L NH_4Cl, and 30 g/L H_3BO_3 and with the following electrodeposition conditions: pH 4.5–5.0, cathodic current density 2 A/dm^2, soluble zinc anodes, and both additives described above.

During electrodeposition, the hybrid samples were prepared in an ultrasonic bath aiming to minimize the influence of the aggregation and to ensure incorporation of uniformly distributed particles into the coatings. To realize credible experimental data for comparison, all the investigated coatings had a thickness of ~12 μm.

2.5. Surface Characterization of the Coatings

For analysis of the structure morphology and chemical composition of the experimental hybrid and ordinary zinc-based coatings, scanning electron microscopy (INCA Energy 350 unit, Oxford Instruments, Oxford, UK), equipped with energy-dispersive X-ray spectroscopy (EDX), was applied.

2.6. Corrosion Characterization

The protective ability of the investigated coatings was evaluated using potentiodynamic polarization curves and polarization resistance measurements. PDP is a well-known accelerated method, while generally Rp measurements are realized for a longer time interval. The electrochemical processes like cathodic electrodeposition and anodic dissolution were investigated by application of cyclic voltammetry (CVA) in the starting electrolytes for the obtaining of hybrid or ordinary zinc coatings. These studies were done using a scan rate of 10 mV/sec in the potential interval between −1.4 V and 0 V. Electrochemical tests were realized with a PAR "VersaStat 4" device. The reference electrode was a saturated calomel electrode (SCE), and a platinum plate was the counter electrode. The state of the tested sample during the PDP test was checked visually by the "naked eye", and after the registration of the low-carbon steel substrate, the external polarization was stopped. The experiments with the Rp method had a duration of 40 days.

2.7. Water Contact Angle Measurements

Water contact angle measurements were carried out with an Easy Drop DSA20E Krűss GmbH apparatus (Hamburg, Germany) at ambient temperature. A sessile droplet of distilled water (10 μL) controlled by a computer-dosing system was deposited onto the samples. Computer analysis of the images of the droplet realized by DSA1 software (v 1.92-05) calculated the WCA. The data were averaged from 5 measurements for each sample.

2.8. XPS Studies

A VG ESCALAB II electron spectrometer was applied for the measurements at conditions of AlKα radiation with an energy of 1486.6 eV. The accuracy of the determining of the binding energies was ±0.1 eV utilizing the C1s line at 285.0 eV (from an adventitious carbon) as a reference. The chemical composition of the films was evaluated on the basis of the areas and binding energies of C1s, O1s, Zn2p, Cl2p, and Na1s photoelectron peaks (after linear subtraction of the background) and Scofield's photoionization cross-sections.

2.9. Test Medium and Reproducibility

A model test medium of 3.5% NaCl solution (pH~6.7) was applied for the realization of the electrochemical-corrosion experiments. The presented results were averaged from the data received from five samples per type, i.e., either ordinary zinc or hybrid zinc coatings.

3. Results

Polyelectrolyte complexes are materials formed via the ionic interaction between oppositely charged polyelectrolytes [38]. In the case of chitosan and alginate, electrostatic interactions between positively charged ($–NH_3^+$) groups of chitosan and negatively charged ($–COO^-$) groups of alginate lead to the production of CHI/ALG nanoparticles with a hydrogel character. Having in mind that the pKa of CHI is 6.5 and the pKa of ALG is about 3.5, a pH 5 of the solutions is accepted to provide optimal conditions for the spontaneous ionic gelation of CHI-TPP and concomitant complexation with ALG [35,37]. The crosslinking agent TPP is used to enhance the water-barrier characteristics of the CHI/ALG hydrogel particles.

The polysaccharide nanoparticles prepared by us are non-stoichiometric polyelectrolyte complexes with an excess of CHI, and their pH-dependent behavior is similar to that of pure CHI. The electrostatic interactions between positively charged molecules of CAF (pKa of CAF is 10.4 [39]) and negatively charged groups of ALG and TPP might explain the CAF entrapment in the CHI/ALG nanoparticles. The interactions between the carbonyl groups of CAF and primary amide groups of CHI are also discussed as a reason for CAF loading into CHI/TPP nanoparticles [40,41].

3.1. Characterization of CHI/ALG Nanoparticles

Under the conditions for the preparation of the CHI/ALG nanoparticles (water solutions with pH 5), the suspensions are stable, and the nanoparticles are positively charged, which favors their electrodeposition on the cathode (steel) surface. The TEM images of CHI/ALG nanoparticles before and after loading with CAF are presented in Figure 2.

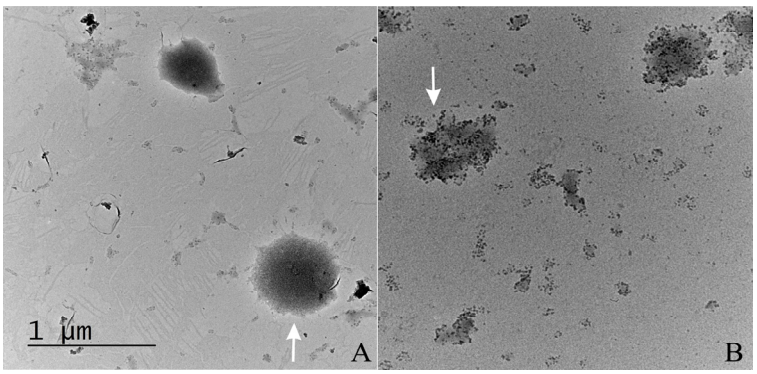

Figure 2. TEM images of CHI/ALG nanoparticles before (**A**) and after (**B**) loading with CAF.

Figure 3A shows the hydrodynamic diameters of the CHI/ALG nanoparticles, both unloaded and loaded with CAF. Here are two families of nanoparticles in both suspensions, obtained after 1 min of sonication. The larger ones show peaks at 326 ± 21 nm and 298 ± 19 nm for unloaded and loaded-with-CAF CHI/ALG nanoparticles, while the smaller particles show peaks at 80 ± 10 nm and 57 ± 6 nm, respectively. This indicates a medium polydispersity of the samples (Table 1), although the suspensions are stable against aggregation as a whole.

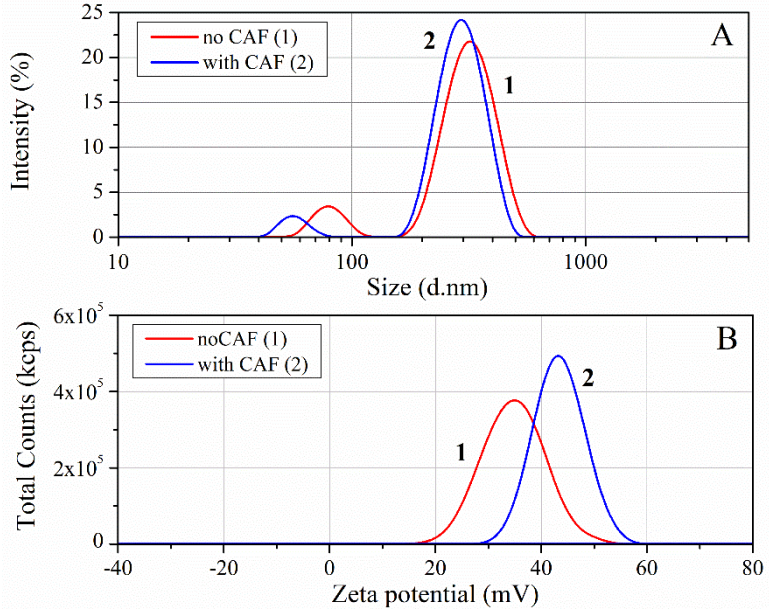

Figure 3. Hydrodynamic diameter distributions (**A**) and zeta potentials (**B**) for the CHI/ALG nanoparticles unloaded and loaded with CAF.

Table 1. Hydrodynamic diameters and zeta potentials of CHI/ALG nanoparticles in water and zinc sulfate electrolyte.

	CHI/ALG *Water Solution*	**CHI/ALG-CAF** *Water Solution*	**CHI/ALG** *Zinc Electrolyte*	**CHI/ALG-CAF** *Zinc Electrolyte*
ζ	+35 ± 5 mV	+43 ± 1 mV	+4.4 ± 3.8 mV	+4.6 ± 4.0 mV
d_1	326 ± 21 nm	298 ± 19 nm	610 ± 60 nm	1640 ± 180 nm
d_2	80 ± 10 nm	57 ± 6 nm	170 ± 8 nm	-
PI	0.25	0.23	0.3	0.35

Figure 3B shows the zeta potential values for both types of nanoparticles. They are +35 ± 5 mV and +43 ± 1 mV for the particles unloaded and loaded with CAF, respectively, which are potentials high enough to provide stabilization of the suspensions [42]. It is interesting to note that the hydrodynamic diameters of the CHI/ALG nanoparticles loaded with CAF are smaller than those of the particles not containing CAF. This could be related to the higher zeta potential values for the particles loaded with CAF, leading to less agglomeration because of the stronger electrostatic repulsions between similar charged nanoparticles.

Bearing in mind that the density of the surface charge of the particles decreases in the bath solution (as a result of the increase in ionic strength), additional measurements of the particles sizes and zeta potentials were carried out in zinc sulfate solutions before electrodeposition of the hybrid zinc coatings. The results presented in Table 1 reveal 2–3 times (and even more) larger hydrodynamic diameters of the particles in the zinc sulfate solution, which is attributed to a significant decrease in their zeta potential values, leading to particle agglomeration. These data are of importance for the analysis of the surface morphology of the coatings on steel substrates.

3.2. Surface Morphology of Hybrid Zinc Coatings on Steel Substrates

The surface morphology of the hybrid zinc coatings obtained by the incorporation of CHI/ALG nanoparticles into the matrix of pure zinc coatings is represented in Figure 4. The SEM images of the coatings demonstrate that the electrodeposition of CHI/ALG nanoparticles without CAF leads to the formation of a coating with large spots of materials with different morphology (Figure 4A). This is better observed at a higher magnification of one spot (inset in Figure 4A), showing a crystalline structure similar to that found in

the investigations of Zhai et al. [43]. According to these authors, large and well-formed crystallographic chitosan–zinc complexes incorporate into the zinc matrix at close to our conditions. When CHI/ALG nanoparticles loaded with CAF are embedded into the zinc coating, the surface morphology differs (Figure 4B). The surface becomes more homogeneous, containing also chitosan—zinc crystals (similar to those in the above coating) and new flat spots related to the availability of CAF (inset in Figure 4B).

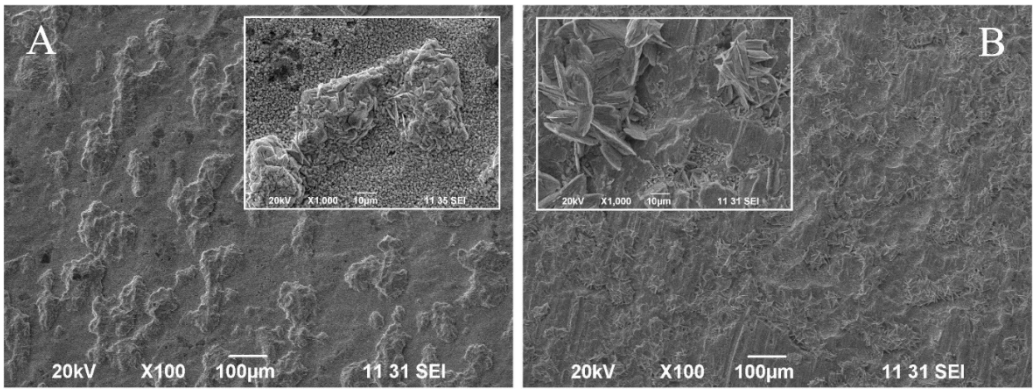

Figure 4. SEM micrographs of hybrid zinc coatings containing CHI/ALG nanoparticles unloaded (**A**) and loaded (**B**) with CAF.

It is interesting to underline that, in the presence of CAF, the coating surface (apart from the chitosan–zinc crystals) contains almost equal amounts of zinc (42 wt%) and iron (47 wt%) (Table 2). In contrast, the EDX analysis of the coating without CAF shows a zinc amount close to 80 wt%. This observation could be regarded as a possible sign that a large number of loaded-with-CAF nanocontainers are electrodeposited directly onto the steel surface.

Table 2. Chemical composition of hybrid zinc coatings (wt.%) before and after treatment in 3.5% NaCl solution.

Spectrum Label	CHI/ALG	CHI/ALG *Treated*	CHI/ALG-CAF	CHI/ALG-CAF *Treated*
C	9.5	5.4	5.8	8.7
N	0.3	0.2	0.0	0.0
O	2.0	22.1	1.5	26.5
Na	5.1	8.2	3.5	8.7
Cl	-	5.3	-	0.8
Fe	3.2	0.8	46.9	2.2
Zn	79.9	58.0	42.3	53.1
Total	100.0	100.0	100.0	100.0

3.3. Entrapment Efficiency and Release of CAF from CHI/ALG Nanoparticles

Using UV–vis spectroscopy, the entrapment efficiency of CAF in the CHI/ALG nanoparticles obtained at pH 5 was evaluated. After centrifugation of the CHI/ALG suspension (at 15,000 rpm for 1 h at 4 °C), the CAF concentration in the supernatant was measured, and the entrapment efficiency was determined by comparing the amounts measured in the supernatant and the initial amount of CAF used for the preparation of the particles loaded with CAF.

A calibration curve for CAF was obtained at λ = 275 nm (Figure 5). The supernatant was diluted five times before measuring to improve the quality of the results. The amount of CAF measured in the supernatant was 0.173 g/L, which means that the entrapped amount of CAF in the CHI/ALG nanoparticles was 0.827 g/L, i.e., entrapment efficiency of 82.7%.

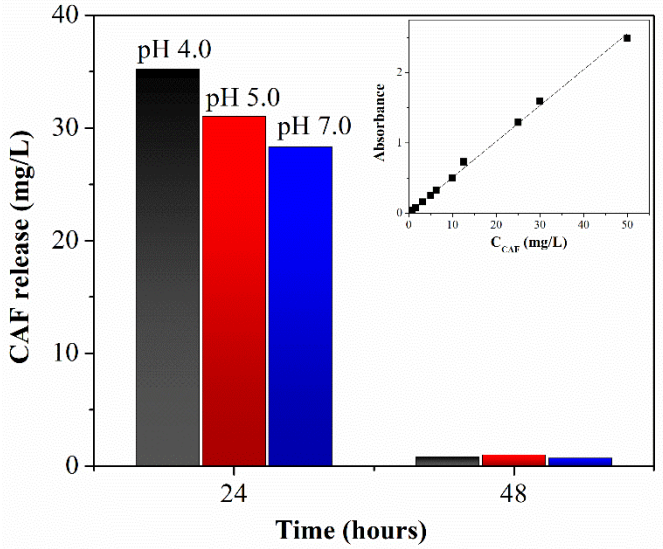

Figure 5. Cumulative release of CAF from CHI/ALG nanoparticles in 3.5% NaCl solutions at pH 7, pH 5, and pH 4. Inset: Calibration curve for CAF.

Since caffeine displays good corrosion inhibition in acidic and neutral conditions [7,8], the release of CAF from the CHI/ALG nanoparticles was measured under neutral (pH 7) and acidic (pH 4 and pH 5) conditions. For the measurements, the precipitated CHI/ALG nanoparticles loaded with CAF were redispersed by sonication in 3.5% NaCl solutions of a defined pH for 1 min. After 24 h, the suspensions were centrifuged (at the above conditions), and the supernatants were collected for UV-vis analysis. The process of centrifugation and redispersion by sonication was repeated, and the cumulative release amounts of CAF after 48 h were calculated. They were equal to 29 mg/L, 32 mg/L, and 36 mg/L for the samples studied at pH 7, 5, and 4, respectively (Figure 5). The results show a higher released amount of CAF at lower pH values, which can be attributed to the increased swelling of the CHI/ALG complexes under acidic conditions [24]. Since the corrosion process has been found to reduce pH in the region close to the zinc layer on steel (due to metal hydrolysis) [44], the increased amount of released CAF at lower pH is expected to provide a more effective protective ability to the coating in the case of a corrosion attack.

In addition, CAF protonates better in acidic solutions [45,46], which enhances the repulsion between positively charged CAF and positively charged CHI (being in excess in our CHI/ALG nanoparticles) to facilitate the CAF release in acidic media. The obtained results indicate that the CHI/ALG nanoparticles loaded with CAF are potential candidates to hinder the corrosion processes of galvanized steel under neutral and acidic conditions. For comparison, similar amounts of CAF have been found to ensure about 95% protection for carbon steel in well water (pH 8.5) in the presence of Zn^{2+} ions (50 ppm of CAF and 50 ppm of Zn^{2+}) [12].

3.4. SEM of Corrosive-Treated Samples

The surface morphology of corrosive-treated hybrid coatings is demonstrated in Figure 6. It is obvious that some differences (better visible at lower magnification) occur in both samples. The surface of the coating without CAF seems more uneven and rough with some protruded zones (Figure 6A). Contrary to this, the surface of the coating with CAF is more uniform, although some areas with small pits are also present. Separate white spheres, most probably part of the embedded nanocontainers, are also registered (Figure 6B). Interestingly, the higher magnifications of the images look very similar—see the insets.

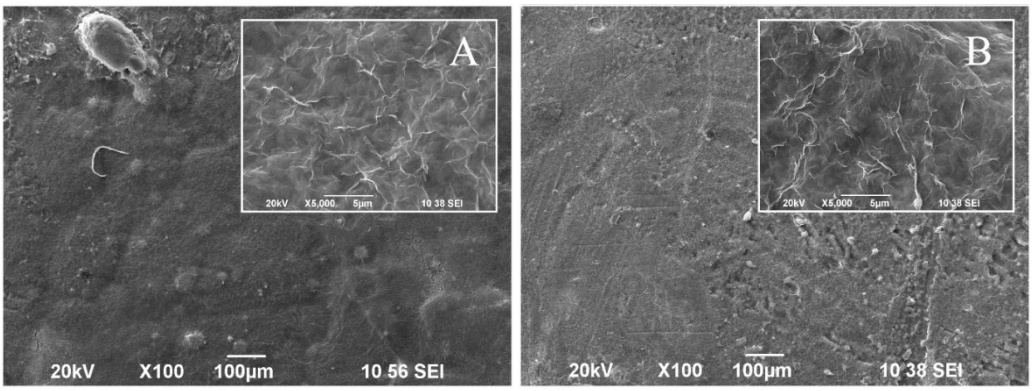

Figure 6. Surface morphology of corrosive-treated hybrid zinc coatings with entrapped CHI/ALG nanoparticles unloaded (**A**) and loaded (**B**) with CAF.

3.5. Measurements with Cyclic Voltammetry

The CVA investigation data of ordinary zinc, as well as of CS and CS CAF samples, are demonstrated in Figure 7A,B. As already mentioned, CVA tests were conducted in the starting electrolytes, from which the ordinary zinc and both hybrid coatings are electrodeposited. Obviously (Figure 7A), the electrodeposition process of the ordinary zinc occurs at a much higher cathodic current (in A): (−0.051) and starts at a more negative potential value compared to both hybrid coatings. This observation is a definite sign that the cathodic process of the zinc proceeds harder (with more difficulties), i.e., the electrodeposition is overpolarized. Contrary to this, the cathodic electrodeposition of both the hybrid coatings investigated takes place at more positive cathodic potentials and lower cathodic currents, i.e., the process is depolarized and is realized easier compared to the ordinary zinc coating. The values of the cathodic currents of the hybrid coatings (which are much lower) are (in A): −0.018 for the CS coating and −0.016 for the CS CAF coating, respectively. It can be calculated that the cathodic electrodeposition peak of the zinc is about three-times higher compared to the CS and CS CAF coatings. In addition, it seems that after the cathodic peaks of CS (in V) (−1.236) and CS CAF (−1.241), the electrodeposition of the hybrid coatings occurs under diffusion control until the vertex potential. This is a sign that in such a case the potential changes do not affect the current values, which for a given potential interval remain unchanged.

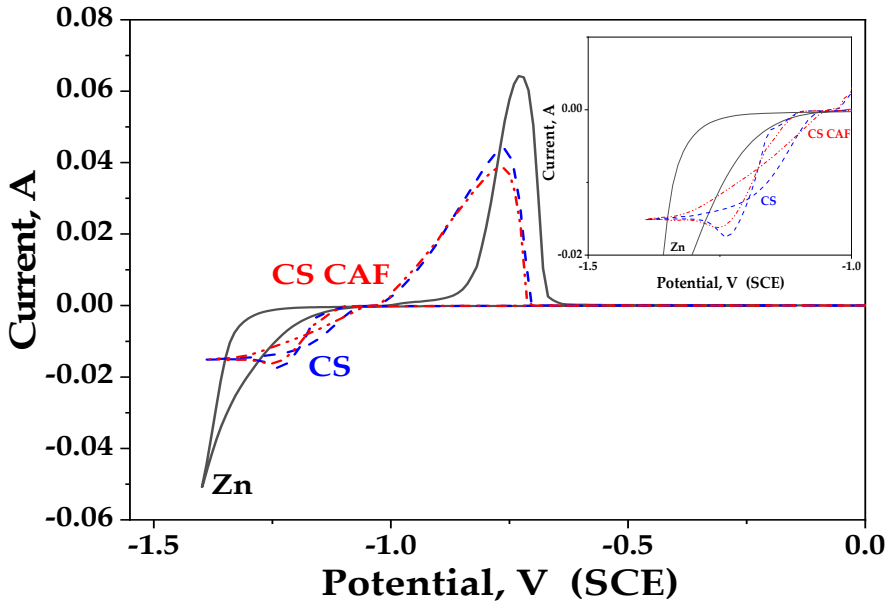

Figure 7. Cyclic voltammetry studies of the investigated coatings in the starting electrolytes.

In the anodic area is presented the dissolution process of the investigated samples. The availability of anodic parts of the CVA curves is proof for the existence of electrodeposited metallic mass (coatings) on the low-carbon steel, which is formed as a result of the cathodic polarization. It is obvious that the zinc dissolution peak is the greatest one (0.065 A at −0.725 V), which indicates the presence of a greater electrodeposited metal quantity. The anodic peaks of both hybrid coatings are much lower (in A), i.e., 0.044 for CS and 0.038 for CS CAF. Figure 7B shows clearly the peculiarities of the occurring cathodic processes.

The availability of CHI/ALG nanoparticles or CHI/ALG nanocontainers with CAF in the starting electrolytes can be regarded as an essential reason for the obtained results. The nanoparticles/nanocontainers are bigger in size compared to the zinc ions and can physically block the substrate for electrodeposition of zinc ions, impeding in such a way the obtaining of the hybrid coatings.

3.6. Potentiodynamic Polarization Curves

The results obtained via the potential polarization method are presented in Figure 8. Generally, this method is applied as an accelerated test and gives the possibility to obtain information about the corrosion behavior of the investigated coatings at external polarization. As shown in Figure 8, the corrosion potential of the ordinary zinc coating is placed at more negative values, i.e., at (in V) −1.07, compared to both hybrid coatings. The corrosion potential (in V) of CS is −1.04 and that of CS CAF is −1.02.

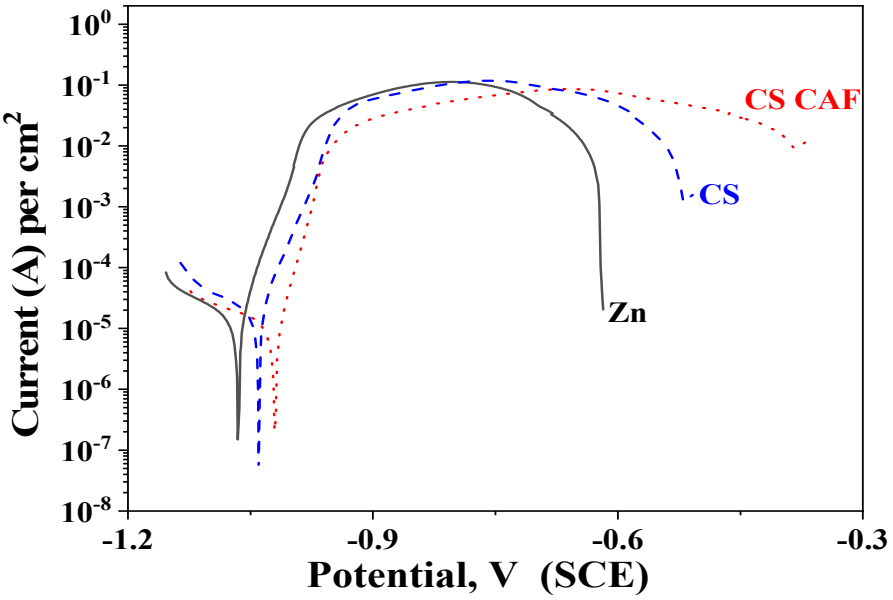

Figure 8. Potentiodynamic polarization curves of the investigated coatings in a model medium of 3.5% NaCl solution.

The corrosion current densities, registered under external polarization, also differ—the I_{corr} of the ordinary zinc coating is higher compared to both hybrid coatings. This is an indication of the accelerated corrosion process of the sample. The zinc anodic curve is growing gradually in the potential area after the corrosion potential demonstrating a maximal value, i.e., a higher anodic current density, at a potential (in V) of about −0.8. Thereafter, this coating is fully dissolute in the potential area of about −0.6 (in V) and as a result the "bare" low-carbon steel surface arises. Contrary to this, both hybrid zinc coatings CS and CS CAF show different behavior. It is obvious that the anodic parts of the hybrids are longer compared to that of the ordinary zinc coating, which is better presented especially for CS CAF. This result confirms that the newly elaborated hybrid coatings are more stable and corrosion resistive at external anodic polarization. The length of the anodic curve (in V) of the CS sample is up to about −0.52 and that of CS CAF is until −0.38. In

the maximal anodic dissolution area, both hybrid samples have relatively lower maximal current densities compared to the same parameter registered for the ordinary zinc coating. Table 3 contains some of the electrochemical indicators taken from the figure.

Table 3. Electrochemical parameters obtained from Figure 8.

Sample	I_{corr}, A·cm^{-2}	E_{corr}, V
Zn	1.6×10^{-5}	−1.07
CS	1.5×10^{-5}	−1.04
CS CAF	1.3×10^{-5}	−1.02

3.7. Measurements of the Polarization Resistance

The experimental data from the polarization resistance measurements after a 40-day period of stay for the tested coatings in a 3.5% NaCl solution are presented in Figure 9. Obviously, the ordinary zinc coating demonstrates the lowest Rp values of about 780–850 ohm·cm^2 during the immersion period. The maximal Rp can be observed after 25 days of investigation.

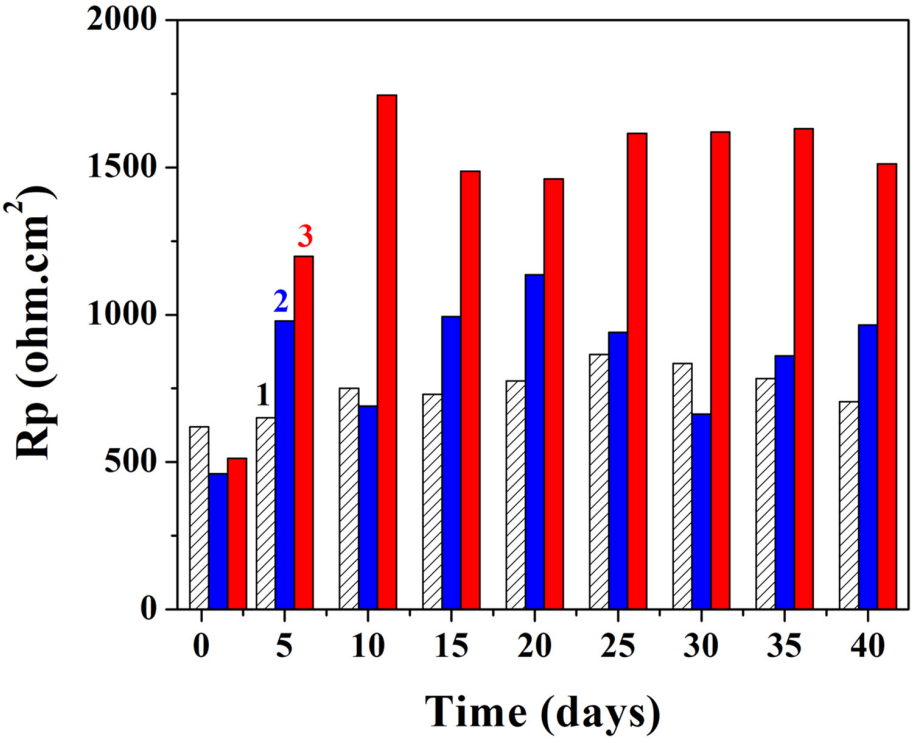

Figure 9. Polarization resistance measurements: 1—ordinary zinc coating; 2—CS; and 3—CS CAF coatings.

Contrary to this, the experimental maximal Rp values for CS (~1150 ohm·cm^2) and CS CAF (~1750 ohm·cm^2) are between 1.5- and 2-times higher. This is a sign that the presence of nanoparticles/nanocontainers in the zinc matrix influences positively the anticorrosion characteristics of the zinc coating, better expressed for the hybrid coating with embedded nanocontainers containing CAF.

3.8. Water Contact Angle Studies

According to many experimental results, a more hydrophobic surface is beneficial for the anticorrosion protection of metal materials. The wettability of both hybrid coatings was estimated by measuring the water contact angle (Figure 10). As observed, the CS coating is less hydrophobic than CS CAF, and it could be supposed that the latter will demonstrate an enhanced resistance against corrosion.

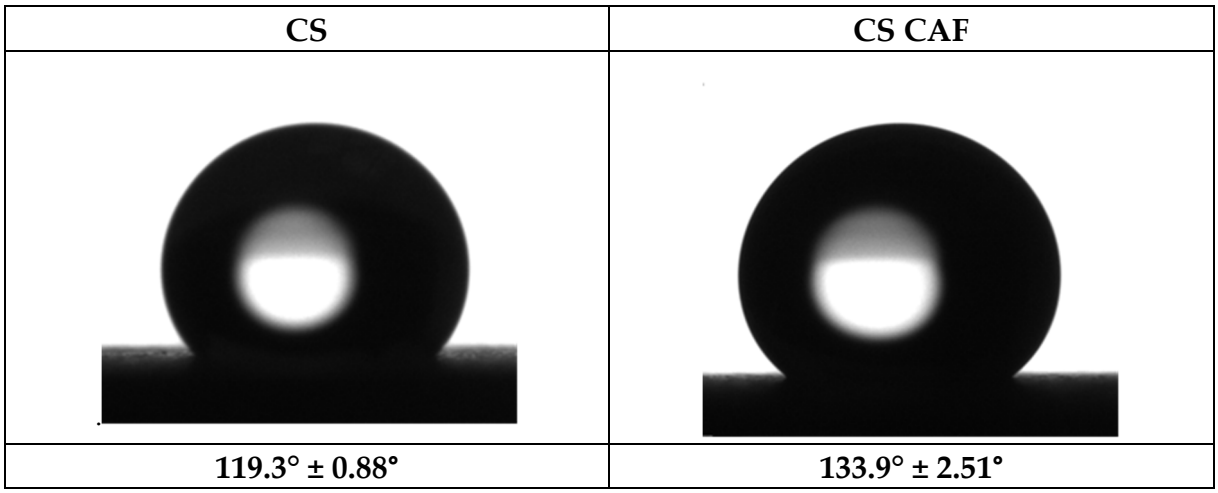

Figure 10. Water contact angle measurements of the investigated coatings: left—CS coating; right—CS CAF coating.

The water contact angles registered have similar values. It is well known that the hydrophobicity of the sample surface is generally determined by both intrinsic chemical properties and surface microstructure. The experimental data on the dependence between hydrophobicity and corrosion resistance are to a certain degree contradictory. However, many scientists support the opinion that this parameter as a rule is a sign for an inhibited corrosion process.

3.9. XPS Studies

An XPS study was used to evaluate the chemical state and amount of chemical elements on the surface of the corrosion-treated hybrid zinc coatings. Several elements like C, O, Zn, Cl, and Na were found on the surface, and their quantity is represented in Table 4. The shape of C1s spectra demonstrates several peaks, which are attributed to adventitious carbon, C-O, carboxyl, and carbonyl groups, respectively. The functional groups are attached to the polymer. The different types of carbon are presented in Table 5. The O1s spectra are wide and consist of three peaks, which can be associated with oxygen in a zinc hydroxide lattice at 531.1 eV and C=O and C-O bond at 532.5 eV and 533.5 eV, respectively (Figure 11). Zn2p spectra have a maximum with a binding energy of 1023.8 eV.

Table 4. XPS results of the composition of hybrid zinc coatings.

Samples	C, at. %	O, at. %	Zn, at. %	Cl, at. %	Na, at. %
CS	22.6	45.4	25.2	6.0	0.8
CS CAF	24.6	45.4	23.3	5.9	0.8

Table 5. The percentages of C from various species.

Binding Energy, eV	Chemical Bonding	Concentration, %	
		CS	CS CAF
285.0	C-C	35.0	49.4
286.1	C-O	29.3	19.3
288.3	COOH	9.0	6.4
290.0	C=O	26.7	24.9

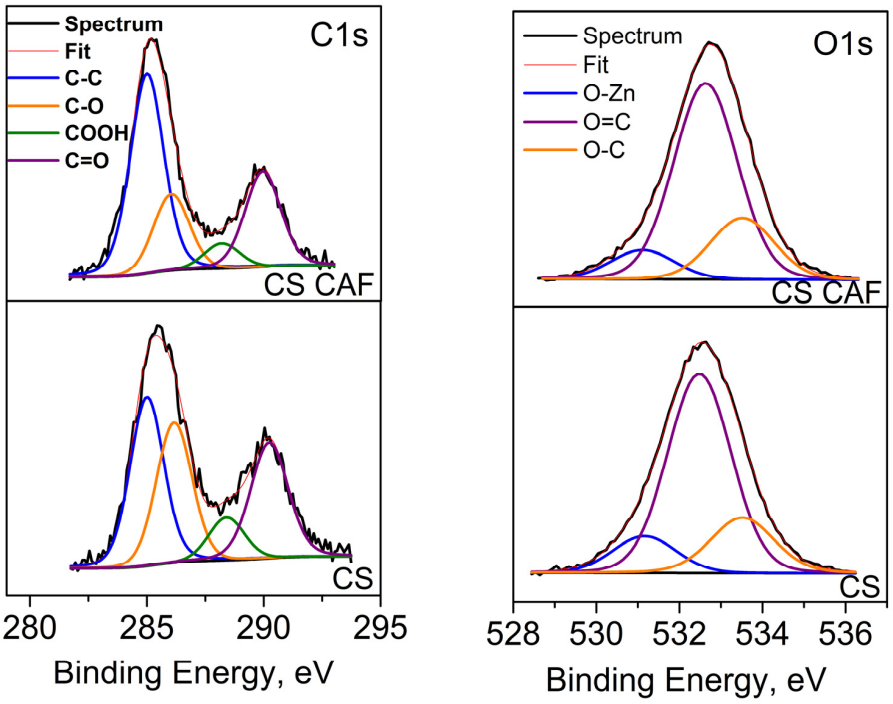

Figure 11. Deconvolution of the C1s and O1s core-level spectra of the hybrid zinc coatings.

The Zn LMM Auger peaks are used to determine the state of zinc. They have a larger shift of chemical state. The modified Auger parameter was calculated, and it showed that the zinc was in the form of $Zn(OH)_2$—which is a part of zinc hydroxyde chloride $Zn_5(OH)_8Cl_2.H_2O$—on the surface (Figure 12):

$$a' = KE_{ZnLMM} + BE_{Zn2p3/2}$$

$$a' = 985.8\ eV + 1023.8\ eV = 2009.6\ eV \Rightarrow Zn(OH)_2$$

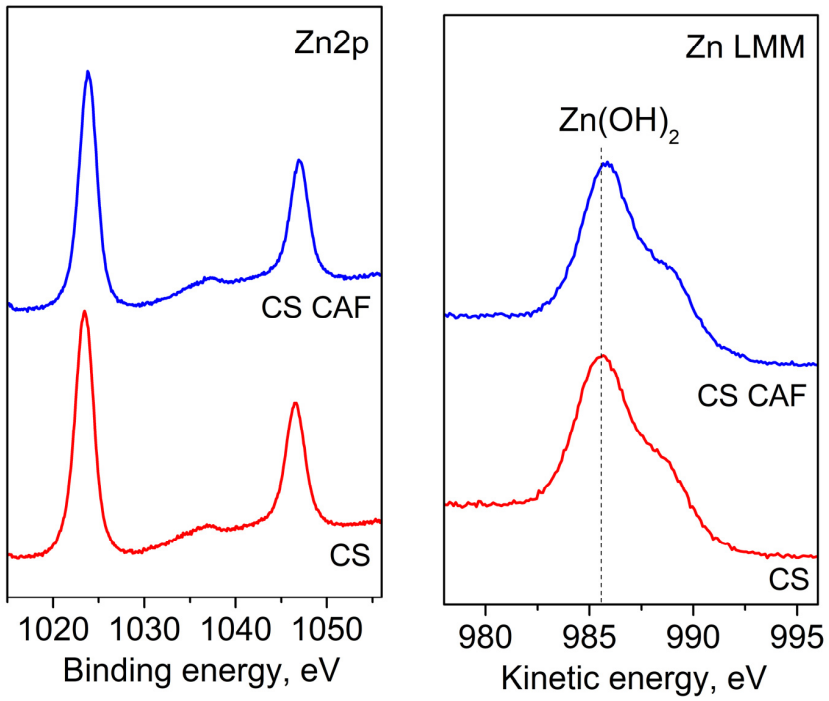

Figure 12. Photoelectron and Auger spectra of the hybrid zinc coatings.

The addition of CAF did not change the shape of the spectra. A small shift to higher binding energies of the order of 0.4 eV is observed, which is probably a result of the different surface charge due to photoemission. On the surface was recorded also Cl and a small amount of Na due to the corrosion treatment in NaCl. The coatings cover the low carbon steel substrate well, and this is evidenced by no iron peaks on the surface [47,48].

4. Discussion

The test data obtained by the application of both hybrid zinc coatings on steel substrates demonstrate similar anticorrosion characteristics and surface composition. The corrosion potential values (E_{corr}) of both hybrid coatings represent positive potential shifts compared to the ordinary zinc coating, i.e., the hybrid coatings are more "noble". In addition, their corrosion current density values, received from the potentiodynamic polarization curves, are lower compared to the ordinary zinc coating, which means that they are more corrosion resistive. It is also obvious that the anodic curves of the hybrid samples are longer than that of the zinc coating, i.e., these systems seem to last more at external anodic polarization conditions. The polarization resistance measurements during a 40-day immersion period confirm the results from the accelerated tests. This result is a sign of the better-expressed corrosion resistance and protective ability of the newly developed hybrid zinc-based coatings.

The results from the conducted investigations can be related to the newly formed corrosive products arising during the tests. According to previous studies, the expected product due to corrosion in such a corrosion medium is zinc hydroxide chloride $Zn_5(OH)_8Cl_2 \cdot H_2O$. Its availability leads to better-expressed protection against corrosion agents forming a protective "barrier" layer. The presence of nanoparticles/nanocontainers in the zinc matrix, on the other hand, influences positively the anticorrosion behavior of the zinc coating. When polymer nanoparticles/nanocontainers are present in the metal matrix, one can suggest that the corrosion process is localized in the metal zones surrounding the nano-objects.

Thereupon, the accelerated destruction of zinc will begin and a "mixed" film of $Zn_5(OH)_8Cl_2 \cdot H_2O$ and the polymeric-based nanoparticles/nanocontainers will appear. Finally, the corrosion process will spread around the nanoparticles, and the probability of the obtaining of local penetrations and sudden destruction deep inside the coating will be minimized. Such a development will increase the probability for the local corrosion to be transformed into a general one, which in turn will decrease the destruction of the coating. In the case of general corrosion, the surface damages are easy to be registered, which allows the prevention to be realized in time.

5. Conclusions

1. Nanoparticles based on chitosan/alginate complexes were loaded with corrosion inhibitor caffeine to obtain environmentally friendly nanocontainers suitable for incorporation into the matrix of a protective zinc coating on mild steel. It was shown that the technique used for the preparation of the nanocontainers allows the entrapment of caffeine at a pH 5 of the initial solutions and pH-dependent release in a model corrosion medium containing 3.5% NaCl.
2. The SEM analysis reveals that the incorporation of caffeine-loaded nanocontainers leads to a more homogeneous surface of the hybrid zinc coating compared to the coating with nanoparticles not loaded with caffeine.
3. CVA studies confirm that the electrodeposition of the hybrid coatings is depolarized compared to the ordinary zinc, i.e., occurs easier.
4. The wettability of the hybrid coating containing caffeine is lower compared to the hybrid coating without the inhibitor, which is a sign of its greater hydrophobicity.
5. The corrosion investigations confirmed the positive influence of the incorporated nanoparticles and nanocontainers on the corrosion stability of the investigated hybrid coatings in the model test medium containing chloride ions as corrosion activators.

Author Contributions: Conceptualization, T.R. and N.B. (Nikolai Boshkov); methodology, K.K., N.B. (Nelly Boshkova) and M.S.; software, M.S.; validation, K.K., N.B. (Nelly Boshkova) and M.S.; formal analysis, M.S.; investigation, N.B. (Nelly Boshkova), K.K. and N.B. (Nikolai Boshkov); resources; data curation, K.K., N.B. (Nelly Boshkova), and M.S.; writing—T.R. and N.B. (Nikolai Boshkov); writing—review and editing, T.R. and N.B. (Nikolai Boshkov); visualization; supervision, N.B. (Nikolai Boshkov); project administration, N.B. (Nikolai Boshkov); funding acquisition. All authors have read and agreed to the published version of the manuscript.

Funding: This research received no external funding.

Data Availability Statement: The data presented in this study are available on request from the corresponding author due to due to privacy.

Acknowledgments: Research equipment of the Distributed Research Infrastructure INFRAMAT, part of the Bulgarian National Roadmap for Research Infrastructures, supported by the Bulgarian Ministry of Education and Science, was used for some investigations in the present study.

Conflicts of Interest: The authors declare no conflicts of interest.

References

1. Boshkov, N. Galvanic Zn-Mn alloys—Electrodeposition, phase composition, corrosion behavior and protective ability. *Surf. Coat. Technol.* **2003**, *172*, 217–226. [CrossRef]
2. Li, M.; Luo, S.; Qian, Y.; Zhang, W.; Jiang, L.; Shen, J. Effect of additives on electrodeposition of nanocrystalline zinc from acidic sulfate solutions. *J. Electrochem. Soc.* **2007**, *154*, D567–D571. [CrossRef]
3. Utu, I.-D.; Muntean, R.; Mitelea, I. Corrosion and wear properties of Zn-based composite coatings. *J. Mater. Eng. Perform.* **2020**, *29*, 5360–5365. [CrossRef]
4. Murphy, E.B.; Wudl, F. The world of smart healable materials. *Prog. Polym. Sci.* **2010**, *35*, 223–251. [CrossRef]
5. Shchukin, D.G.; Möhwald, H. Surface-engineered nanocontainers for entrapment of corrosion inhibitors. *Adv. Funct. Mater.* **2007**, *17*, 1451–1458. [CrossRef]
6. Zheludkevich, M.I.; Tedim, J.; Ferreira, M.G.S. Smart coatings for active corrosion protection based on multifunctional micro and nanocontainers. *Electrochim. Acta* **2012**, *82*, 314–332. [CrossRef]
7. Saji, V.S. Supramolecular concepts and approaches in corrosion and biofouling prevention. *Corros. Revc.* **2019**, *37*, 187–230. [CrossRef]
8. Zhang, Y.; Yu, M.; Chen, C.; Li, S.M.; Liu, J.H. Self-healing coatings based on stimuli-responsive release of corrosion inhibitors: A review. *Front. Mater.* **2022**, *8*, 795397. [CrossRef]
9. Srivastava, M.; Srivastava, S.K.; Ji, G.; Prakash, R. Chitosan based new nanocomposites for corrosion protection of mild steel in aggressive chloride media. *Int. J. Biol. Macromol.* **2019**, *140*, 177–187. [CrossRef]
10. Da Trindade, L.G.; Gonçalves, R.S. Evidence of caffeine adsorption on a low-carbon steel surface in ethanol. *Corr. Sci.* **2009**, *51*, 1578–1583. [CrossRef]
11. De Souza, F.S.; Gonçalves, R.S.; Spinelli, A. Assessment of caffeine adsorption onto mild steel surface as an eco-friendly corrosion inhibitor. *J. Braz. Chem. Soc.* **2014**, *25*, 81–90. [CrossRef]
12. Elmsellem, H.; Aouniti, A.; Youssoufi, M.H.; Bendaha, H.; Benhadda, T.; Chetouani, A.; Warad, I.; Hammouti, B. Caffeine as a corrosion inhibitor of mild steel in hydrochloric acid. *Phys. Chem. News* **2013**, *70*, 84–90.
13. Grosser, F.N.; Goncalves, R.S. Electrochemical evidence of caffeine adsorption on zinc surface in ethanol. *Corr. Sci.* **2008**, *50*, 2934–2938. [CrossRef]
14. De Souza, F.S.; Giacomelli, C.; Gonçalves, R.S.; Spinelli, A. Adsorption behavior of caffeine as a green corrosion inhibitor for copper. *Mater. Sci. Eng.* **2012**, *32*, 2436–2444. [CrossRef]
15. Rajendran, S.; Amalraj, A.J.; Joice, M.J.; Anthony, N.; Trivedi, D.C.; Sundaravadivelu, M. Corrosion inhibition by the caffeine—Zn^{2+} system. *Corros. Rev.* **2004**, *22*, 233–248. [CrossRef]
16. Kulig, D.; Zimoch-Korzycka, A.; Jarmoluk, A.; Marycz, K. Study of alginate-chitosan complex formed with different polymers ratio. *Polymers* **2016**, *8*, 167. [CrossRef]
17. Shaari, N.; Kamarudin, S.K. Chitosan and alginate types of bio-membrane in fuel cell application: An overview. *J. Power Sourc.* **2015**, *289*, 71–80. [CrossRef]
18. Abdul Khalil, H.P.S.; Saurabh, C.K.; Adnan, A.S.; Fazita, M.N.; Syakir, M.I.; Davoudpour, Y.; Rafatullah, M.; Abdullah, C.K.; Haafiz, M.K.; Dungani, R. A review on chitosan-cellulose blends and nanocellulose reinforced chitosan biocomposites: Properties and their applications. *Carbohydr. Polym.* **2016**, *150*, 216–226.
19. Deepa, B.; Abraham, E.; Pothan, L.A.; Cordeiro, N.; Faria, M.; Thomas, S. Biodegradable nanocomposite films based on sodium alginate and cellulose nanofibrils. *Materials* **2016**, *9*, 50. [CrossRef] [PubMed]
20. Umoren, S.A.; Eduok, U.M. Application of carbohydrate polymers as corrosion inhibitors for metal substrates in different media: A review. *Carbohydr. Polym.* **2016**, *140*, 314–341. [CrossRef]

21. Obot, I.B.; Ikenna, B.; Onyeachu, A.; Kumar, M. Sodium alginate: A promising biopolymer for corrosion protection of APIX60 high strength carbon steel in saline medium. *Carbohydr. Polym.* **2017**, *178*, 200–208. [CrossRef] [PubMed]
22. Simsek-Ege, F.A.; Bond, G.M.; Stringer, J. Polyelectrolye complex formation between alginate and chitosan as a function of pH. *J. Appl. Polymer Sci.* **2003**, *88*, 346–351. [CrossRef]
23. Gierszewska, M.; Ostrowska-Czubenko, J.; Chrzanowska, E. pH-responsive chitosan/alginate polyelectrolyte complex membranes reinforced by tripolyphosphate. *Eur. Polym. J.* **2018**, *101*, 282–290. [CrossRef]
24. Niculescu, A.G.; Grumezescu, A.M. Applications of chitosan-alginate-based nanoparticles—An up-to-date review. *Nanomaterials* **2022**, *12*, 186. [CrossRef]
25. Kania, H. Corrosion and Anticorrosion of Alloys/Metals: The important Global Issue Coatings. *Coatings* **2023**, *13*, 216. [CrossRef]
26. Zhang, X.G. *Corrosion and Electrochemistry of Zinc*; Plenum Press: New York, NY, USA, 1996; ISBN 978-1-4757-9877-7.
27. Lide, D.R. (Ed.) *CRC Handbook of Chemistry and Physics*, 90th ed.; Taylor and Francis Group LLC.: Boca Raton, FL, USA, 2010.
28. Porter, F. *Corrosion Resistance of Zinc and Zinc Alloys*, 1st ed.; Taylor & Francis Inc.: Oxfordshire, UK, 1994.
29. Bachvarov, V.; Peshova, M.; Vitkova, S.; Boshkov, N. Corrosion properties of Zn-Ni-P alloys in neutral model medium. *Cent. Eur. J. Chem.* **2014**, *12*, 1183–1193. [CrossRef]
30. Sorensen, P.A.; Kiil, S.; Dam-Johansen, K.; Weinell, C.E. Anticorrosive coatings: A Review. *J. Coat. Technol. Res.* **2009**, *6*, 135–176. [CrossRef]
31. Zhang, H.; Chen, B.; Banfield, J.F. Particle size and pH effects on nanoparticle dissolution. *J. Phys. Chem. C* **2010**, *114*, 14876–14884. [CrossRef]
32. Azizi, M.; Schneider, W.; Plieth, W. Electrolytic co-deposition of silicate and mica particles with zinc. *J. Solid State Electrochem.* **2005**, *9*, 429–437. [CrossRef]
33. Xia, X.; Zhitomirsky, I.; McDermid, J.R. Electrodeposition of zinc and composite zinc-yttria stabilized zirconia coating. *J. Mater. Process. Technol.* **2009**, *209*, 2632–2640. [CrossRef]
34. Adriana, V.; Simona, V.; Aurel, P.; Caius, B.; Liana, M.M. Electrodeposited Zn–TiO_2 nanocomposite coatings and their corrosion behavior. *J. Appl. Electrochem.* **2010**, *40*, 1519–1527.
35. Goycoolea, F.M.; Lollo, G.; Remunan-Lopez, C.; Quaglia, F.; Alonso, M.J. Chitosan-alginate blended nanoparticles as carriers for the transmucosal delivery of macromolecules. *Biomacromolecules* **2009**, *10*, 1736–1743. [CrossRef] [PubMed]
36. Leonardi, M.; Caruso, G.M.; Carroccio, S.C.; Boninelli, S.; Curcuruto, G.; Zimbone, M.; Allegra, M.; Torrisi, B.; Ferlito, F.; Miritello, M. Smart nanocomposites of chitosan/alginate nanoparticles loaded with copper oxide as alternative nanofertilizers. *Environ. Sci. Nano* **2021**, *8*, 174–187. [CrossRef]
37. Boshkova, N.; Kamburova, K.; Radeva, T.; Simeonova, S.; Grozev, N.; Boshkov, N. Hybrid zinc coatings with chitosan/alginate encapsulated CuO-nanoparticles for anticorrosion and antifouling protection of mild steel. *Coatings* **2023**, *13*, 895. [CrossRef]
38. Thunemann, A.F.; Muller, M.; Dautzenberg, H.; Joanny, J.F.; Löwen, H. Polyelectrolyte complexes. *Adv. Polym. Sci.* **2004**, *166*, 113–171.
39. Rigueto, C.V.T.; Nazari, M.T.; De Souza, C.F.; Cadore, J.S.; Briao, V.B.; Piccin, J.S. Alternative techniques for caffeine removal from wastewater: An overview of opportunities and challenges. *J. Water Process Eng.* **2020**, *35*, 101231. [CrossRef]
40. Abu Hassan, N.A.F.; Sahudin, S.; Hussain, Z.; Hussain, M. Self-assembled chitosan nanoparticles for percutaneous delivery of caffeine: Preparation, characterization and in vitro release studies. *Int. J. Appl. Pharm.* **2018**, *10*, 172–185. [CrossRef]
41. Abosabaa, S.A.; El Meshad, A.N.; Arafa, M.G. Chitosan nanocarrier entrapping hydrophilic drugs as advanced polymeric system for dual pharmaceutical and cosmeceutical application: A comprehensive analysis using Box-Behnken design. *Polymers* **2021**, *13*, 677. [CrossRef]
42. Meissner, T.; Oelschlagel, K.; Potthoff, A. Implications of the stability behavior of zinc oxide nanoparticles for toxicological studies. *Int. Nano Lett.* **2014**, *4*, 116–129. [CrossRef]
43. Zhai, X.; Sun, C.; Li, K.; Guan, F.; Liu, X.; Duan, J.; Hou, B. Synthesis and characterization of the chitosan-zinc composite electrodeposits with enhanced antibacterial properties. *RSC Adv.* **2016**, *6*, 46081–46088. [CrossRef]
44. Dutra, C.A.M.; Codaro, E.N.; Nakazato, R.Z. Electrochemical behavior and corrosion study of electrodeposits of Zn and Zn-Fe-Co on steel. *Mater. Sci. Appl.* **2012**, *3*, 348–354.
45. Bahrami, H.; Tabrizchi, M.; Farrokhpour, H. Protonation of caffeine: A theoretical and experimental study. *Chem. Phys.* **2013**, *415*, 222–227. [CrossRef]
46. Andrade, M.B.; Santos, T.R.T.; Guerra AC, S.; Silva, M.F.; Demiti, G.M.M.; Bergamasco, R. Evaluation of magnetic nano adsorbent produced from graphene oxide with iron and cobalt nanoparticles for caffeine removal from aqueous medium. *Chem. Eng. Proc. Process Intensif.* **2022**, *170*, 108694. [CrossRef]
47. Winiarski, J.; Tylus, W.; Winiarska, K.; Szczygieł, I.; Szczygieł, B. XPS and FT-IR Characterization of Selected Synthetic Corrosion-Products of Zinc Expected in Neutral Environment Containing Chloride Ions. *Hindawi J. Spectrosc.* **2018**, 2079278.
48. Biesinger, M.C.; Lau, L.W.M.; Gerson, A.R.; Smart, R.S.C. Resolving surface chemical states in XPS analysis of first row transition metals, oxides and hydroxides: Sc, Ti, V, Cu and Zn. *Appl. Surf. Sci.* **2010**, *257*, 887–898. [CrossRef]

Disclaimer/Publisher's Note: The statements, opinions and data contained in all publications are solely those of the individual author(s) and contributor(s) and not of MDPI and/or the editor(s). MDPI and/or the editor(s) disclaim responsibility for any injury to people or property resulting from any ideas, methods, instructions or products referred to in the content.